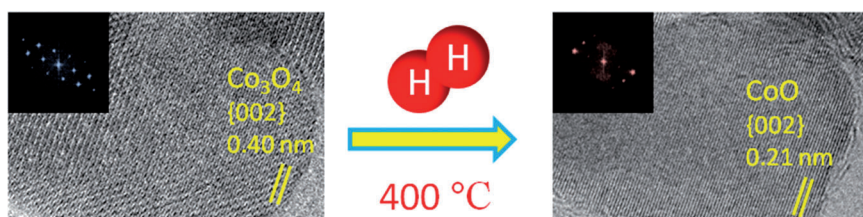


FULL PAPERS



*M. R. Ward, E. D. Boyes, P. L. Gai**

■ ■ - ■ ■

**In Situ Aberration-Corrected
Environmental TEM: Reduction of
Model Co_3O_4 in H_2 at the Atomic Level**



Co_3O_4 reduction is CoO: By using advanced aberration-corrected environmental TEM, the intricacies of the dynamic atomic scale reduction of Co_3O_4 in H_2 that are of interest in hydrogenation reactions, such as the Fischer–

Tropsch process, have been investigated. Notably, the transformation process at low pressure proceeds via an advancing interface between Co_3O_4 and CoO regions. Co metal is observed at higher pressure.

DOI: 10.1002/cctc.201300047

In Situ Aberration-Corrected Environmental TEM: Reduction of Model Co_3O_4 in H_2 at the Atomic Level

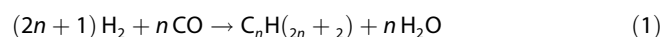
Michael R. Ward, Edward D. Boyes, and Pratibha L. Gai*^[a]

Understanding the dynamic evolution of structural changes in catalysts at the atomic level under controlled reaction conditions is one of the most challenging areas in heterogeneous catalysis. Here we present aberration-corrected environmental TEM at the atomic level and electron diffraction of the reduction of model Co_3O_4 catalysts in H_2 to directly observe the dynamic phase evolution in the reduction process. New insights into the reduction of Co_3O_4 to the intermediate CoO include the formation of an advancing atomic scale interface between

Co_3O_4 and CoO regions. The interface penetrates further into the Co_3O_4 crystal, with the CoO regions replacing the previous Co_3O_4 structure, with increasing reduction. The reduction to CoO proceeds at approximately 200 °C at rounded edges containing atomic steps on the surfaces. The interfaces are observed in crystals larger than approximately 15 nm in size but not in smaller crystals, which indicates the rapid reduction of smaller nanoparticles. The most dramatic changes are observed at 350 °C in larger crystals of size 50 nm.

Introduction

Supported Co-based nanoparticles are of interest in a number of hydrogenation reactions, such as the Fischer–Tropsch (F–T) process for synthetic fuel technologies, and in environmental control. The F–T process contains a series of chemical reactions involving the hydrogenation of CO over catalysts that produce various hydrocarbons according to Equation (1):

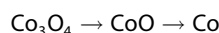


in which n is an integer. The above reaction is a surface-catalysed polymerisation reaction.^[1] The Fe-based catalysts are reported to be selective towards alkanes in the C_{1-4} range at a high temperature of 350 °C and a pressure of 25 mbar (2.5 kPa).^[2] The Co-based catalysts have been used because they offer a compromise between cost, efficiency and selectivity for linear hydrocarbons at a low temperature of 225 °C.^[3] The Co-based catalysts have been found to be highly selective towards C_{5+} hydrocarbons, which is beneficial for the synthesis of diesel.^[3] On the basis of chemical methods and activity measurements, active sites in the F–T process have been reported to be Co^0 (Co metal).^[3] Typical F–T catalysts use Co nanoparticles on supports such as Al_2O_3 ; however, the metal loading can often be above 33% to encourage a high level of activity and selectivity.^[4]

Promoter effects have been reported in Co-based catalysts, which lead to an increase in the active site concentrations.^[5-7] The model Co on carbon nanofibres suggests that the specific activity of C_{5+} molecules decreases as the nanoparticle size decreases below 7 nm with an increase in the C_{1-3} molecule selectivity.^[8,9] The same group have also observed that the support is inert whereas more common supports such as Al_2O_3 can form mixed oxides with the supported nanoparticle species.^[8,9]

The uncertainties surrounding the activity of Co-based catalysts may originate from their activation processes. Co is rarely available as a pure metal for the development of catalysts. Instead, an oxide, usually Co_3O_4 ,^[10,11] is reduced through pretreatment in H_2 and N_2 . The nature of the reduction of the oxide ultimately determines the range of reduced/oxidised Co species in the catalyst. These species play a key role in the structure, morphology and activity of the catalyst.

Both ex situ and in situ studies have revealed a two-stage reduction process of Co_3O_4 .^[12-16]



in which Co has a structure that is size dependent,^[17] with smaller particles of size <30 nm favouring the face centred cubic (fcc) phase. CoO is always observed in its rock salt phase unless special sample preparations are used.^[18,19] The unit cells for the three common fcc forms of Co_3O_4 , CoO and Co are shown in Figure 1.

Exceptions to the above reduction sequence have been observed by different groups. By using in situ XRD, Bulavchenko et al.^[13] showed that at high H_2 pressures [1 atm (101.3 kPa)], the intermediate CoO phase is not observed on unsupported Co_3O_4 and Co (hexagonal close packed) forms directly from Co_3O_4 . In gas mixtures in which H_2 partial pressure is low

[a] M. R. Ward,[†] Prof. E. D. Boyes,[†] Prof. P. L. Gai*
The York-JEOL Nanocentre
University of York
Heslington, York YO10 5DD (UK)
E-mail: pratibha.gai@york.ac.uk

[†] All authors belong to the Department of Physics, Prof. E. D. Boyes to the Department of Electronics and Prof. P. L. Gai to the Department of Chemistry.

Supporting information for this article is available on the WWW under <http://dx.doi.org/10.1002/cctc.201300047>.

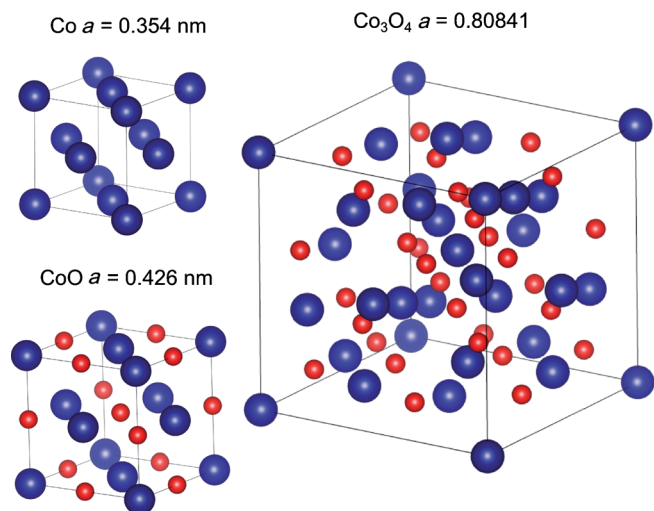


Figure 1. Unit cells of cubic Co, rock salt CoO and spinel Co_3O_4 as labelled. The models are approximately to scale. The larger blue balls are Co, and the smaller red ones are O. Models were generated by using the VESTA program.

[1 Torr (133.3 Pa) of 10% H_2/N_2] and at 400 °C, Li et al.^[20] reported that Co is not observed in the in situ nanoanalysis with high-angle annular dark field scanning transmission electron microscopy studies, and similar conclusions were reported in XRD studies by Bulavchenko et al.^[13] Conventional HRTEM has shown that the reduction process is epitaxial between Co (cubic), CoO and Co_3O_4 ,^[12,14] and the support increases the reduction temperature owing to metal–support interactions.^[13,15]

Dehghan et al.^[12] investigated the change in the structure of a promoted 20 wt.% Co/0.5 wt.% Re/ Al_2O_3 catalyst at 3.4 mbar (0.34 kPa) up to 360 °C by using in situ environmental TEM. They found that Co metal forms at 360 °C and CoO at temperatures as low as 150 °C. The promoter Re is believed to encourage the reduction of CoO to Co.^[21]

To better understand the complex phase evolution at the atomic level in the dynamic reduction of cobalt oxides initially in H_2 , we used model Co_3O_4 catalysts. And, understanding the reduction of model catalysts can lead to deeper insights into the operation of real catalysts. There are relatively few dedicated dynamic atomic scale electron microscopy studies on unsupported model Co_3O_4 catalysts. By using conventional TEM [ex situ post-reaction studies on samples treated at 1 atm (101.3 kPa)], Potoczna-Petru and Kepinski^[14] suggested that CoO and Co form on the crystals larger than 40 nm in size, which possibly causes stacking faults and voids to appear in the remaining Co_3O_4 structure. They reported that high-temperature reduction (> 400 °C) can result in the formation of Co at the surface, which causes any CoO formed to reduce in an autocatalytic fashion. Because this experiment was performed ex situ, there appears to be no consensus on the possible formation of stacking faults and their relationship to the reduction mechanism. Such defects were not observed by Dehghan et al.^[12] Dieckmann^[22] reported that there were no reliable data on the defect structure of Co_3O_4 ; however, Casas-Cabanas et al.^[23] showed that Co atoms can occupy interstitial sites in

Co_3O_4 , which leads to unusual intensities in {111} and {220} reflections.

Here we have investigated the intricacies of the reduction of Co_3O_4 to CoO at the atomic level under controlled low H_2 pressure and at elevated temperatures by using aberration-corrected environmental TEM (AC-ETEM) developed in-house by Gai and Boyes.^[24–26] Our aim is to directly observe and identify the process by which Co_3O_4 transforms to reduced phases in crystals of different sizes. Our observations have revealed that the evolution of CoO starts at approximately 200 °C primarily at Co_3O_4 crystal edges composed of low-symmetry facets. The transformation process is gradual, which always contains an interface between Co_3O_4 and CoO regions. We observed defects only in crystals larger than 30 nm in size, with Co_3O_4 present up to approximately 450 °C, whereas particles less than approximately 20 nm in size transformed completely to CoO by 400 °C. The atomic level insights into the dynamic reduction of the model catalysts presented here are important to understand the dynamic behaviour and activity of real supported Co-based catalysts in hydrogenation reactions and will be useful in the future catalyst design.

Results and Discussion

In situ reduction HRTEM and diffraction sequences

Dynamic AC-ETEM images and the corresponding fast-Fourier transform (FFT) patterns of reaction sequences of a Co_3O_4 catalyst crystal at different temperatures during exposure to H_2 in situ are shown in Figure 2. Co_3O_4 was readily identified from other phases because of the presence of a large 0.47 nm {111} atomic plane spacing. In the FFT, the {002} forbidden reflections are present, which indicates double diffraction. The crystal shown in Figure 2a at room temperature is rounded on the right-hand side, which indicates the presence of low-symmetry atomic planes that contain kinks and steps. Kinks and steps act as nucleation sites and encourage the adsorption and breaking of H–H bonds on Pt.^[27] Potoczna-Petru and Kepinski^[14] also suggested that rounded Co_3O_4 crystals are more likely to contain defects on the surface. They referred to the work of Paryjczak et al.,^[15] in which the synthesis temperature of the Co_3O_4 crystals affected the onset of the reduction to CoO and the synthesis temperature correlated with the nature of crystal facets.

Increasing the temperature to 150 °C resulted in no structural changes in our observations. At approximately 200 °C, the initial signs of structural changes were observed. The image in Figure 2b indicates that the crystal region previously with a rounded edge as in Figure 2a has become more faceted. The new surface is terminated by CoO {002}. It is not a perfect surface and has some residual steps present (arrowed). The FFT shows distorted Co_3O_4 {002} and {004} reflections. The two reflections are in the vicinity of each other, which indicates some “broadening” of the reflections. The two closely spaced reflections indicate the presence of CoO that has {002} spacings within 1% of Co_3O_4 {004}. The CoO region formed on the surface penetrates approximately 3.4 nm into the Co_3O_4 crystal.

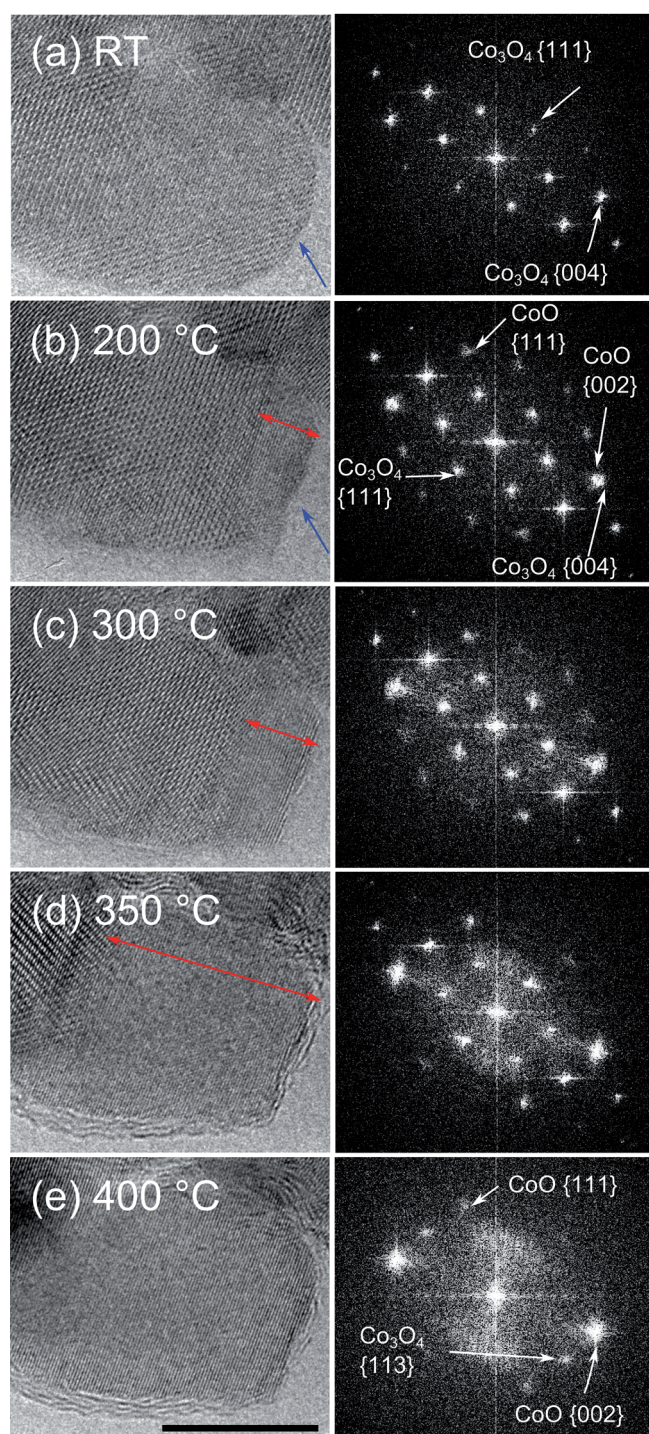


Figure 2. Dynamic aberration-corrected environmental TEM image sequence with the corresponding FFTs in H_2 gas as a function of reaction temperature, showing the reduction of Co_3O_4 to CoO at the temperatures indicated. The FFT in (a) shows Co_3O_4 ; in (b)–(d) the Co_3O_4 {004} reflections have become broad because of the similar CoO {002} spacing. In (e), the FFT shows just CoO with the Co_3O_4 originating from another crystal. The blue arrow shows that the rounded edge of the crystal has become flat after heating and the red arrow shows dimensions of the CoO region. Scale bar in image e is 10 nm.

This is approximately six unit cells of CoO . The FFT indicates that the lattice parameter varies across this region and that there is an interface between the modified edge and the rest

of the Co_3O_4 structure. By allowing for the 6% difference between Co_3O_4 and a doubled CoO unit cell, the mismatch could lead to strain relaxation in this region.

Increasing the temperature up to $300^\circ C$ caused the CoO region to grow and penetrate deeper into the Co_3O_4 crystal whilst maintaining an essentially epitaxial grain boundary, which is similar to the observation at $200^\circ C$. The distance it penetrated into the Co_3O_4 crystal was 6.1 nm at $300^\circ C$, which is double that of at $200^\circ C$. Although the FFT in Figure 2c was obtained from the region around the boundary, separate FFTs (not shown) confirmed that the left-hand side of the crystal is CoO . At this temperature, we also observed similar events occurring primarily at the edges of other rounded, differently sized crystals. In contrast, flat facets (e.g. {111} and {200}) remained unchanged during the reduction process. There seems to be a correlation between low-symmetry faces and the reduction-onset temperature, which is consistent with previous reports.^[14]

At $350^\circ C$, there is a dramatic change in the contrast of crystals. The CoO region has moved further into the Co_3O_4 crystal, and the penetration is 15 nm deep. On the left-hand side of the crystal, dramatic contrast can be observed. The previous images suggest that there are multiple crystals here with slight orientation differences between them. The unusual contrast seen on the left-hand side of the image (and elsewhere) could be due to double diffraction. The FFT demonstrates no additional spacings, which suggests that the effects observed are the Moiré fringes. The Moiré fringe width D can be calculated by using Equation (2).

$$D = d_1 d_2 / [(d_1 - d_2)^2 + d_1 d_2 \theta^2] \quad (2)$$

in which d_1 and d_2 are the atomic plane distances for each species responsible for the Moiré fringes and θ is the angle between them. The Moiré fringes in Figure 2d generate effects in $[\bar{1}11]$ and $[1\bar{3}1]$ directions. The Moiré fringes are caused by the overlap of the strong CoO {002} planes in the smaller crystal and the Co_3O_4 {113} planes in the large parent crystal.

At $400^\circ C$, the crystal that was initially Co_3O_4 (as shown in Figure 2a) is now completely CoO (as shown in Figure 2e). The surrounding region is also CoO . The Moiré fringe contrast seen at $350^\circ C$ was also observed at $400^\circ C$ but only in regions larger than 30 nm in size. The larger crystals had structures resembling a core-shell structure, and CoO was the shell and Co_3O_4 the core. The resultant overlap produced Moiré fringes in the central regions of crystals larger than 20 nm in size. This was not observed on smaller crystals, because the CoO transformation was much more rapid.

Increasing the temperature up to $500^\circ C$ resulted in no discernible change in the structure, which suggested that the low H_2 pressure is insufficient to facilitate the reduction of CoO . Our results are consistent with the observations of Bulavchenko et al.^[13] at low H_2 partial pressure, who observed that Co was not formed.

The observations of Potoczna-Petru and Kepinski^[14] suggested that Co metal is formed in the middle of the modified structures; however, by using in situ microscopy, Dehghan et al.^[12]

showed that richer oxides were prevalent at the edges because of residual O atoms re-oxidising CoO and Co to Co_3O_4 and CoO, respectively, after H_2 was removed from their microscope and cooled overnight.

Nanoparticles less than 15 nm in size were observed to completely reduce to CoO at a lower temperature of 350 °C. An example is shown in the AC-ETEM images and the corresponding FFTs (Figure 3), which illustrates a spherical nanoparticle approximately 12 nm in size. The crystal in Figure 3a has stepped surfaces; however, the observations indicate that even after reduction, the stepped surfaces remain. In small particles

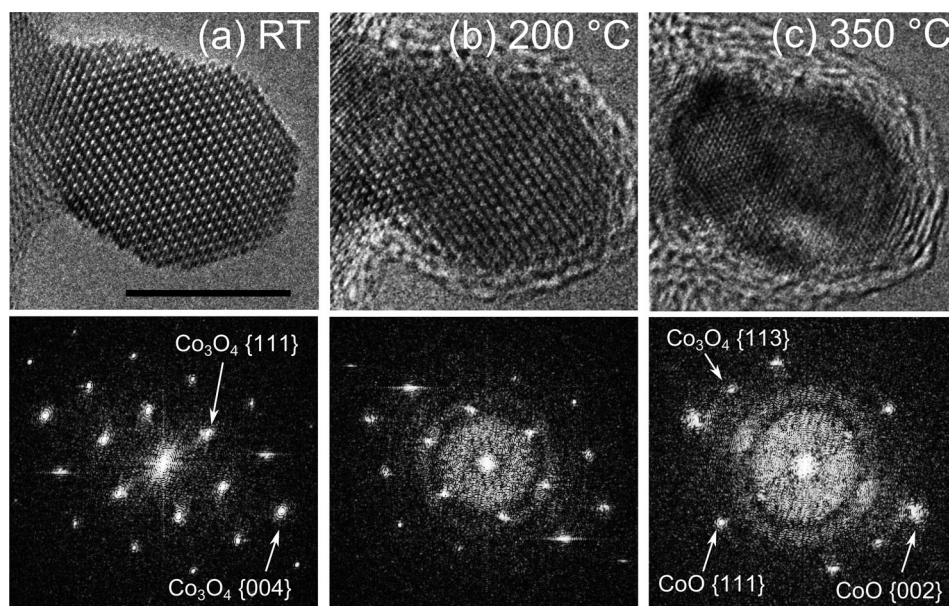


Figure 3. Dynamic aberration-corrected environmental TEM image sequence in H_2 gas as a function of the reaction temperature with corresponding FFTs of a Co_3O_4 nanocatalyst approximately 12 nm in size. The particle transforms completely to CoO at 350 °C, but the larger nanoparticle it is connected to is still primarily Co_3O_4 . The surrounding amorphous layer is carbonaceous and is probably due to the contamination on the nearby Cu grid bar. The scale bar in image a is 10 nm.

(≈ 2 nm), the removal of low coordinated surface atoms to minimise the surface energy and transport of the atoms between particles leads to sintering and faceting.^[28] It is possible that in the larger particle shown in Figure 3, primary faceting has already occurred. In general, Co_3O_4 particles larger than 20 nm in size, irrespective of their initial shape, became more faceted as they were reduced to CoO.

In Figure 4a, the ETEM image shows the central region of a Co_3O_4 crystal with a maximum width of approximately 50 nm. A sequence of the corresponding selected area electron diffraction patterns at the temperatures indicated and the evolution of reflections due to the reduction are shown in Figure 4b–e. There are no major changes at temperatures below 300 °C except for a slight change in the orientation of the crystal, which results in small differences in the diffracted intensities.

At 300 °C, weak CoO reflections can be identified in the diffraction pattern. The differences in reciprocal lattice vectors are more apparent for the higher-order reflections (e.g. Co_3O_4

{444} and CoO {222}). As in the cases in Figures 2 and 3, the Co_3O_4 and CoO crystallographic directions are essentially epitaxial, with no clear rotation between the two crystals; that is, {002} and {111} faces between the two materials are parallel to each other.

Notably, although there are no major structural changes up to 300 °C, the Co_3O_4 {111} planes gradually lose their intensity at the expense of other Co_3O_4 {004} and CoO {002} reflections. Electron diffraction intensities can vary as a function of crystal thickness, but also because of the tilt of the crystal with respect to the beam. The diffraction patterns shown in Figure 3

are approximately between 3 and 5° away from the exact [110] zone axis. The structure factor for spinel materials predicts that {440} reflections should be the most intense, followed by {113}, {400} and {115} reflections. At 300 °C, the most intense reflections are the {400} reflections followed by {113} reflections. By using JEMs, which is an HRTEM image simulation package, and our aberration-corrected electron microscope parameters (given in Table S1), we simulated the electron diffraction patterns shown in Figures S1 and S2. They indicate that any major difference between predicted and observed intensities can be due to the crystal tilt rather than the presence of point defects as reported by Casas-Cabanas et al.^[23]

The Co_3O_4 {004} reflections become significantly brighter and broader at 400 °C, which indicates the occurrence of bulk transformations to CoO. By 450 °C, the transformation is complete and the crystal has orientated itself closer to the CoO [110] zone axis, which leads to more typical intensities in different reflections.

Co_3O_4 to CoO transformation mechanism

In dynamic in situ reduction process at the atomic level, an interface boundary is formed in most crystals. A close-up of such an interface is shown in Figure 5. The crystal shown in Figure 5 is away from the [110] zone axis by approximately 4°. The tilt is such that one set of the {111} reflections is the strongest in the FFT and diffraction patterns and thus {111} planes dominate in the image.

To understand the origin of the dark contrast observed between the Co_3O_4 {111} planes at the top of Figure 5 and to explore the presence of Co_3O_4 and CoO including the effect of tilt on the contrast, JEMS image simulation package was used. By using the Laue circle tool, it is possible to add tilt before

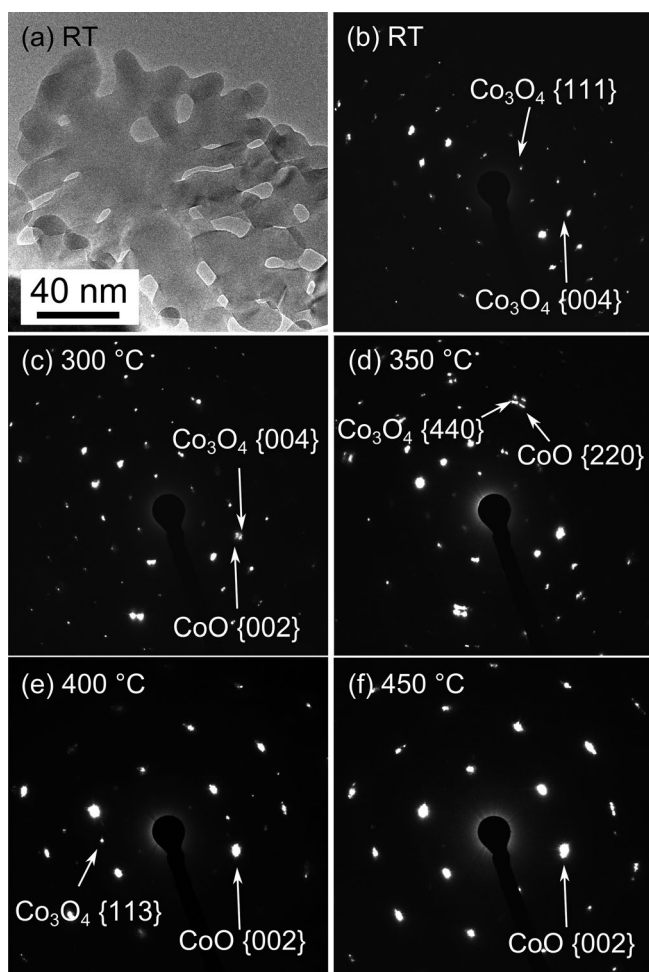


Figure 4. Dynamic selected area electron diffraction sequence in which frame a is an aberration-corrected environmental TEM image of the area. With the increase in temperature, the CoO reflections become more dominant and the Co_3O_4 reflections disappear at 450°C . The 500°C pattern is not shown because it is virtually identical to that of 450°C , which implies that no Co is formed.

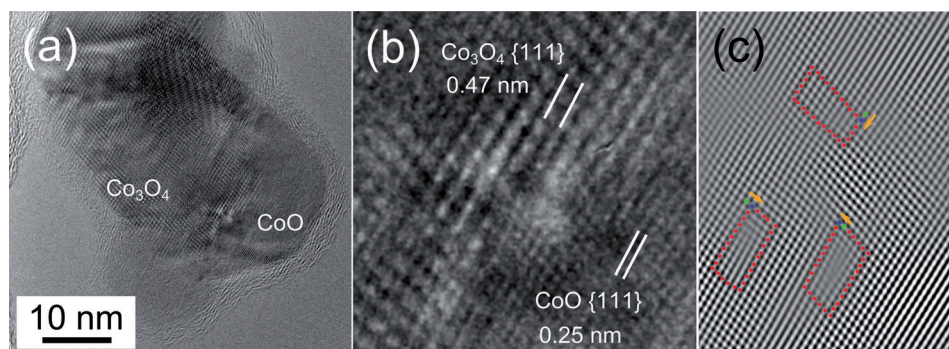


Figure 5. AC-ETEM images of the interface between Co_3O_4 and CoO regions: a) at low magnification and b) at high magnification. TEM simulations show that the contrast seen at the top of image b can be due to the effect of thickness and defocus. The contrast in the central region in image b (which is the area around the interface) indicates the presence of defects. The defects (dislocations) are revealed through the filtration of the Co_3O_4 {222} reflections as shown in image c in the FFT (not shown). The green and blue dots in image c signify the start and end of the Burger's circuit, respectively. Preliminary analysis suggests that the dislocations have Burger's vector of the type $\frac{1}{2}[110]$.

image calculations by using Co_3O_4 (ICSD 28158^[29]) and CoO (ICSD 624575) [110] HRTEM images using settings corresponding to our AC-ETEM images. The width of the crystal varies between 25 and 30 nm; therefore, we used this as the thickness of the crystal for simulations. Our simulations have shown that the dark contrast is due to the effect of thickness and defocus (Figure S3).

In smaller Co_3O_4 crystals, the rapid transformation to CoO is accompanied by the loss of surface O atoms and the formation of anion vacancy sites at the surface that can provide highly active sites for the dissociation of H_2 . The lattice parameter of Co_3O_4 is 0.8084 nm, and the lattice parameter of CoO is 0.426 nm, as shown in Figure 1. By allowing for the doubling of CoO unit cell, there is still approximately 6% mismatch between the two structures. Our preliminary analysis of Figure 5b and its filtered image shown in Figure 5c reveals the presence of dislocations around the interface boundary that can accommodate the strain at the interface due to the mismatch in the transformation and indicates $\frac{1}{2}[110]$ Burger's (displacement) vector for the defects. The existence of interfaces between rock salt and spinel materials and in materials with small lattice mismatch has been reported, for example between MgO and Fe_3O_4 ^[30] and between NiO and Fe_3O_4 ^[31] in which the lattice mismatch is less than 1%. At these interface boundaries, anti-phase boundaries (and not dislocations) have been reported. In bimetallic metal nanoparticles, such as Pt–Pd nanoparticles in which Pd and Pt have lattice parameters within 1%, stacking faults and dislocations have been observed.^[28]

CoO to Co transformation

During a scouting experiment using a higher pressure [3 mbar (0.3 kPa) inlet pressure], Co metal (fcc) formed at 450°C . The AC-ETEM images illustrating Moiré fringes caused by the overlap of the parallel CoO and Co {111} planes are shown in Figure 6a. In Figure 6a, Co is limited to the Moiré fringe regions as revealed by the filtration of the image by masking the Co {111} reflections. Co metal forms small clusters on the crystals and eventually spreads forming a Co shell. The Co shell was also observed in another crystal shown in Figure 6b at 450°C , in which the Moiré fringes have become more extensive.

Conclusions

We have presented direct atomic level insights into the dynamic reduction of model Co_3O_4 catalysts in controlled H_2 environments at elevated temperatures. The observations have revealed that the transformation in crystals larger than approximately 20 nm in size proceeds gradually

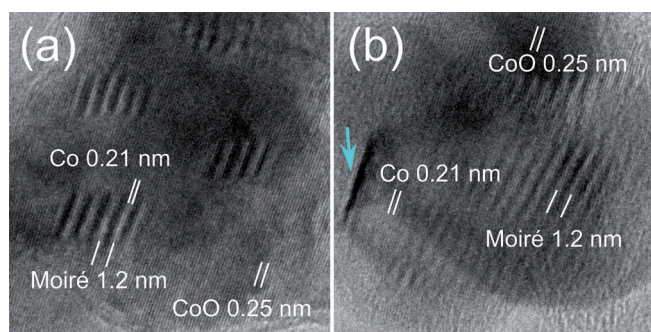


Figure 6. Aberration-corrected environmental TEM images obtained at 450 °C and during a separate experiment with a pressure 3 times greater than that in the previous experiments. In this case, we observed the formation of Co metal on the surfaces in clusters at this high temperature. The blue arrow in image b indicates a defect. Filtered FFT images show that there are several dislocations near the yellow arrow, and the strained region could be responsible for the dark contrast.

with an atomic interface between Co_3O_4 and CoO regions, which penetrates deeper into the crystal with the increase in temperature. The formation of CoO is observed to proceed at 200 °C but only at the edges of rounded crystals, which suggests that the weakly bound O should be removed from the surface so to create surface sites for the dissociation of H_2 . The observation of CoO at operating temperatures of approximately 200–350 °C has important implications in understanding the catalytic activity of Co-based oxides used in hydrogenation reactions.

The observations of Co metal at higher temperatures of 450 °C and at higher pressures (≈ 3 times used at which only CoO is observed) suggest that higher temperature and higher pressure are required for the transformation.

Experimental Section

The Co_3O_4 powder was obtained from Aldrich. TEM and selected area electron diffraction analysis of the powder showed primarily Co_3O_4 .

Specimens for conventional electron microscopy analysis were prepared by dispersing a small amount of Co_3O_4 powder in ethanol, which was then treated in an ultrasonic bath for 2 min. The solution was then deposited on to holey C grids. For in situ ETEM studies, unfiled (empty) Cu grids were used because C films buckle at high temperatures and react with samples under H_2 at elevated temperatures. The empty Cu grids were plasma-cleaned at 75% power for 5 min with a Diener/Femto plasma cleaner to remove any contamination. After depositing the Co_3O_4 powder, the specimens were further plasma cleaned at 10% power for 30 s. Crystals protruding over the edge of the grids were used in the in situ studies.

For dynamic real-time in situ studies at the atomic level under controlled gas and temperature conditions, we used a double AC-E TEM developed in-house by Boyes and Gai^[24–26] in the Nanocentre at the University of York. The AC-E TEM with sub-angstrom (< 100 pm) resolution was developed by modifying a double aberration-corrected JEOL 2200FS (S)TEM operating at 200 kV, which was fitted with a large-gap objective lens pole piece and gas-tolerant

pumping system.^[24–26] This in-house AC-E TEM development followed the pioneering development of atomic resolution ETEM by Gai and Boyes.^[32,33]

This AC-E TEM enabled gas to be injected into the microscope, and in the current stages of testing the pressure at the sample was approximately 0.1 mbar (0.01 kPa). The removal of aberrations from the objective lens means that it is possible to operate the microscope with the highest resolution without the need for through-focal series, which is essential for real-time atomic resolution dynamic in situ studies. The AC-E TEM has a large objective lens pole-piece, which enables the following holders to be used: A Gatan 628 single-tilt heating holder was used for in situ experiments. A standard JEOL double-tilt holder was also used, but because of the large-gap pole piece, tilts up to 25° in the X and Y axes were possible.^[34]

Careful in situ studies were performed with low electron beam to minimise any beam effects, and the data were verified with calibration blank studies without the beam by using methods reported previously.^[24–26] Several dynamic experiments were performed with sample areas away from the electron beam to minimise exposure, and the areas were periodically checked under the beam at different temperatures. Several minutes were allowed for temperatures to stabilise. The temperature was increased in 50 °C steps up to 500 °C. We believe that the injection of gas into the specimen chamber can cause a cooling effect on the thermocouple of the heating holder. We repeated this experiment several times and found that for a given current the temperature varied by a few degrees.

A JEOL 2011 TEM was also used for specimen screening. Dark-field TEM was used to image defects in Co_3O_4 . This was performed by placing the in situ reduced sample into a double-tilt holder for post-reduction analysis.

Acknowledgements

P.L.G. thanks the journal and the guest editors Prof. Dangsheng Su and Prof. R. Schlogl for the invitation to contribute to this Special Issue on Electron Microscopy for Catalysis. We thank the Engineering and Physical Sciences Research Council, UK, for the research funding and for a PhD studentship for M.R.W.

Keywords: aberration-corrected environmental TEM • cobalt • electron diffraction • Fischer–Tropsch • heterogeneous catalysis

- [1] a) C. K. Rofer-DePoorter, *Chem. Rev.* **1981**, *81*, 447–474; b) A. Datye et al., *Ind. Chem. Res.* **2003**, *42*, 4001.
- [2] A. P. Steynberg, R. L. Espinoza, B. Jager, A. C. Vosloo, *Appl. Catal. A* **1999**, *186*, 41–54.
- [3] E. Iglesia, *Appl. Catal. A* **1997**, *161*, 59–78.
- [4] R. Oukaci, A. H. Singleton, J. G. Goodwin, *Appl. Catal.* **1999**, *186*, 129–144.
- [5] G. J. Haddad, B. Chen, J. J. G. Goodwin, *J. Catal.* **1996**, *161*, 274–281.
- [6] M. Rothaemel, K. F. Hanssen, E. A. Blekkan, D. Schanke, A. Holmen, *Catal. Today* **1997**, *38*, 79–84.
- [7] F. Rohr, O. A. Lindvåg, A. Holmen, E. A. Blekkan, *Catal. Today* **2000**, *58*, 247–254.
- [8] G. L. Bezemer, U. Falke, A. J. van Dillen, K. P. de Jong, *Chem. Commun.* **2005**, 731–733.
- [9] G. L. Bezemer, J. H. Bitter, H. P. C. E. Kuipers, H. Oosterbeek, J. E. Holewijn, X. Xu, F. Kapteijn, A. J. van Dillen, K. P. de Jong, *J. Am. Chem. Soc.* **2006**, *128*, 3956–3964.

- [10] S. E. Colley, R. G. Copperthwaite, G. J. Hutchings, S. P. Terblanche, M. M. Thackeray, *Nature* **1989**, 339, 129–130.
- [11] H. Schulz, *Appl. Catal. A* **1999**, 186, 3–12.
- [12] R. Dehghan, T. W. Hansen, J. B. Wagner, A. Holmen, E. Rytter, Ø. Borg, J. C. Walmsley, *Catal. Lett.* **2011**, 141, 754–761.
- [13] O. A. Bulavchenko, S. V. Cherepanova, V. V. Malakhov, L. S. Dovlitova, A. V. Ishchenko, S. V. Tsybulya, *Kin. Catal.* **2009**, 50, 192–198.
- [14] D. Potoczna-Petru, L. Kepinski, *Catal. Lett.* **2001**, 73, 41–46.
- [15] T. Paryjczak, J. Rynkowski, S. Karski, *J. Chromatogr. A* **1980**, 188, 254–256.
- [16] H.-Y. Lin, Y.-W. Chen, *Mater. Chem. Phys.* **2004**, 85, 171–175.
- [17] O. Kitakami, H. Sato, Y. Shimada, F. Sato, M. Tanaka, *Phys. Rev. B* **1997**, 56, 13849–13854.
- [18] R. W. Grimes, K. P. D. Lagerlof, *J. Am. Ceram. Soc.* **1991**, 74, 270–273.
- [19] K. M. Nam, J. H. Shim, D.-W. Han, H. S. Kwon, Y.-M. Kang, Y. Li, H. Song, W. S. Seo, J. T. Park, *Chem. Mater.* **2010**, 22, 4446–4454.
- [20] P. Li, J. Liu, N. Nag, P. A. Crozier, *Appl. Catal. A* **2006**, 307, 212–221.
- [21] K. M. Cook, S. Poudyala, J. T. Millerb, C. H. Bartholomewa, W. C. Hecker, *Appl. Catal. A* **2012**, 449, 69–80.
- [22] R. Dieckmann, *Solid State Ionics* **1984**, 12, 1–22.
- [23] M. Casas-Cabanas, G. Binotto, D. Larcher, A. Lecup, V. Giordani, J.-M. Tarascon, *Chem. Mater.* **2009**, 21, 1939–1947.
- [24] P. L. Gai, E. D. Boyes, *Microsc. Res. Tech.* **2009**, 72, 153–64.
- [25] P. L. Gai, E. D. Boyes, *J. Phys.* **2010**, 241, 012055–012060.
- [26] P. L. Gai, E. D. Boyes, *Handbook on Nanoscopy, Vol. 1 and 2* (Eds.: G. Van Tendeloo, D. Van Dyke, S. J. Pennycook), Wiley, **2012**.
- [27] G. A. Somorjai, D. W. Blakely, *Nature* **1975**, 258, 580–583.
- [28] M. R. Ward, T. Hyde, E. D. Boyes, P. L. Gai, *ChemCatChem* **2012**, 4, 1622–1631.
- [29] W. L. Smith, A. D. Hobson, *Acta Crystallogr. Sect. B* **1973**, 29, 362–363.
- [30] V. K. Lazarov, M. Weinert, S. A. Chambers, M. Gajdardziska-Josifovska, *Phys. Rev. B* **2005**, 72, 195401.
- [31] A. Rečnik, D. L. Carroll, K. A. Shaw, D. M. Lind, M. Rühle, *J. Mater. Res.* **1997**, 12, 2143–2151.
- [32] P. L. Gai, K. Kourtakis, *Science* **1995**, 267, 661.
- [33] E. D. Boyes, P. L. Gai, *Ultramicroscopy* **1997**, 67, 219.
- [34] N. Shiju, K. Yoshida, E. D. Boyes, D. R. Brown, P. L. Gai, *Catal. Sci. Technol.* **2011**, 1, 413–425.

Received: January 18, 2013

Published online on ■ ■ ■, 0000